Journal of Computational Physics **151,** 114–134 (1999)
Article ID jcph.1998.6171, available online at http://www.idealibrary.com on IDEAL®

The Nosé–Poincaré Method for Constant Temperature Molecular Dynamics

Stephen D. Bond,* Benedict J. Leimkuhler,* and Brian B. Laird†

*Department of Mathematics and †Department of Chemistry, University of Kansas, Lawrence, Kansas 66045

Received July 6, 1998; revised November 23, 1998

We present a new extended phase space method for constant temperature (canonical ensemble) molecular dynamics. Our starting point is the Hamiltonian introduced by Nosé to generate trajectories corresponding to configurations in the canonical ensemble. Using a Poincaré time-transformation, we construct a Hamiltonian system with the correct intrinsic timescale and show that it generates trajectories in the canonical ensemble. Our approach corrects a serious deficiency of the standard change of variables (Nosé–Hoover dynamics), which yields a time-reversible system but simultaneously destroys the Hamiltonian structure. A symplectic discretization method is presented for solving the Nosé–Poincaré equations. The method is explicit and preserves the time-reversal symmetry. In numerical experiments, it is shown that the new method exhibits enhanced stability when the temperature fluctuation is large. Extensions are presented for Nosé chains, holonomic constraints, and rigid bodies.

I. INTRODUCTION

Molecular dynamics computer simulation [1, 2] has become a standard tool in computational biophysics and chemistry. Traditional molecular dynamics samples configurations from a constant energy or microcanonical distribution. This is often inappropriate because experiments are usually performed at constant temperature (canonical ensemble). Although Monte Carlo methods can be used for the canonical ensemble, these methods cannot be used to recover dynamical quantities and time-correlated functions. Hybrid methods using stochastics with molecular dynamics [3] can be used to generate the correct distributions, but they fail to provide correct dynamical quantities due to the discontinuous, stochastic changes in the flow. Methods using *ad hoc* nonreversible temperature controls [4] and isokinetic constraints [5–7] have also been proposed in the literature. These methods succeed in producing smooth trajectories, but they fail to yield the correct canonical fluctuations in the kinetic energy [1]. This paper will focus on the newer dynamical methods derived from the

0021-9991/99 $30.00

extended Hamiltonian proposed by Nosé [8, 9]:

$$\mathcal{H}_{\text{Nosé}} = \sum_i \frac{\tilde{p}_i^2}{2m_i s^2} + V(q) + \frac{\pi^2}{2Q} + \tilde{g}kT \ln s. \tag{1}$$

Here $\tilde{g} = N_f + 1$, where N_f is the number of degrees of freedom of the real system. The constants T and k are temperature and Boltzmann's constant, respectively. An extended position variable, s, is introduced along with its canonical momenta, π. The constant Q represents an artificial "mass" associated with s. One should note that $\tilde{p}$ is the canonical momenta assosciated with the position variable, q. The tilde is used to distinguish it from the from the real momenta given by $p = \tilde{p}/s$.

Nosé proved that this system generates configurations from the canonical ensemble, provided that the dynamics is ergodic. He also showed that the intrinsic time variable must be rescaled to provide trajectories at evenly spaced points in real time. Using data at unevenly spaced points in time does not cause any difficulties in the computation of ensemble averages, but it does significantly affect the computation of correlation functions. This difficulty is traditionally resolved using a real-variable formulation of the equations called Nosé–Hoover [9, 10]. In this approach, the equations of motion are reformulated using a noncanonical change of variables. (Note that, in this paper, the word canonical has two different meanings depending on context. With respect to statistical mechanical distributions, canonical refers to constant temperature, whereas a canonical change of variables is one that leaves the form of Hamilton's equations invariant.) Although the Nosé–Hoover equations produce canonically distributed configurations, and the dynamics evolve with respect to real time, the resulting system is not Hamiltonian. It does have a conserved quantity which is similar to energy, but the equations of motion do not arise from a corresponding Poisson bracket (see [11, p. 320]). Although the flow is time-reversible, it does not have a canonical *symplectic structure*.

The importance of time reversibility and symplecticness in numerical integrators has recently become a popular topic of discussion [12, 13]. A Hamiltonian system is time-reversible if it is an even function of the momenta, which is the case in classical molecular dynamics. One says the flow of a canonical Hamiltonian system is symplectic because the solution operator preserves the wedge product of differentials, $dp \wedge dq = \sum dp_i \wedge dq_i$. In other words, the sum of oriented areas formed by projections of a 2-surface in phase space onto the $p_i q_i$ coordinate planes is a first integral of the flow [14]. Recently a volume-preserving generalization of the Nosé–Hoover method has been proposed [15]. Although this was a significant achievement, one should note that symplecticness is a stronger property than the (phase space) volume preservation provided by Liouville's theorem. It is only in the special case of one degree of freedom systems that symplecticness is equivalent to area or volume conservation.

For a numerical integrator the symplectic property has important consequences. A numerical method is a discrete map (actually a family of maps parameterized by a stepsize Δt) which can be viewed as a transformation of phase space. If one step of the method maps the point (q^n, p^n) to (q^{n+1}, p^{n+1}), then the method is symplectic if $dp^n \wedge dq^n = dp^{n+1} \wedge dq^{n+1}$. One can apply backward error analysis to symplectic methods designed to approximate the dynamics of Hamiltonian systems [16, 17]. In this case it can be shown that the numerical solution is the *exact solution* of a "nearby" Hamiltonian system, up to an exponentially small error. The Hamiltonian corresponding to the nearby system is obtained in the form of an asymptotic expansion.

Time-reversal symmetry and symplecticness are both strong geometric properties of the flow of a dynamical system. However, time-reversal symmetry of a numerical method does not, in general, provide an approximate conserved energy integral obtainable through an asymptotic expansion, as is available for symplectic methods [17]. Near conservation of energy over long time intervals is a direct result of this approximately conserved quantity. Although time-reversible methods will show the same type of stability near the symmetry plane ($p = 0$), there is no guarantee that this will be the case far from the symmetry plane (at high temperatures) [18]. In addition to stability issues, the use of algorithms which are volume-preserving *and* time-reversible is required for hybrid Monte Carlo methods [19].

In this paper we will show that it is possible to derive a time-reversible, real-time formulation without sacrificing the symplectic structure. This approach uses a new extended Hamiltonian which we call *Nosé–Poincaré*,

$$\mathcal{H} = \left(\sum_i \frac{\tilde{p}_i^2}{2m_i s^2} + V(q) + \frac{\pi^2}{2Q} + gkT \ln s - \mathcal{H}_0 \right) s. \tag{2}$$

Now the constant $g = N_f$, the number of degrees of freedom of the real system. This Hamiltonian system is related to the Nosé system through a Poincaré transformation of time [20–22]. The value of the constant $\mathcal{H}_0$ is chosen such that $\mathcal{H}$ is zero when evaluated at the initial conditions. We will also show that the dynamics of the Nosé–Poincaré system can be integrated explicitly using a symplectic, time-reversible integrator.

In Section II we discuss the Nosé–Hoover approach to reformulating the Nosé Hamiltonian in real variables. We review two of the numerical methods which have been previously proposed for solving the Nosé–Hoover equations [1, 23–25]. In Section III we introduce a new symplectic, time-reversible integrator for Nosé–Poincaré. We verify that it generates configurations from the correct distribution and formulate an appropriate numerical method for propagating the dynamics. Using numerical experiments in Section IV, we compare the Nosé–Poincaré method with two popular methods for Nosé–Hoover. These experiments indicate that the Nosé–Poincaré method has better stability properties in simulations with large fluctuations of the thermostat variable, s. This situation arises when the extended "mass," Q, is made small to increase sampling speed or when the initial conditions are not properly equilibrated to the simulation temperature. In the appendices we discuss the extensions of the Nosé–Poincaré approach to Nosé chains, holonomic constraints, and rigid bodies.

II. THE NOSÉ HAMILTONIAN AND NOSÉ–HOOVER METHOD

Although the Nosé Hamiltonian generates configurations from the canonical distribution, it also introduces an unnatural scaling of the intrinsic time. This introduces computational difficulties, because the configurations are not available at equally spaced points in real time. A real-variable reformulation of the equations of motion was proposed by Nosé [8, 9] to remedy this problem. Simplifications to the real-variable system, resulting in the traditional treatment of the Nosé Hamiltonian called Nosé–Hoover, were proposed by Hoover [10]. In this section we review the Nosé–Hoover system of equations and discuss some of the common numerical methods [1, 23–25] proposed for solving them.

We begin with the equations of motion derived from the Nosé Hamiltonian (1),

$$\frac{dq_i}{d\tau} = \frac{\tilde{p}_i}{m_i s^2}, \qquad \frac{ds}{d\tau} = \frac{\pi}{Q}, \tag{3}$$

$$\frac{d\tilde{p}_i}{d\tau} = -\frac{\partial}{\partial q_i} V(q), \qquad \frac{d\pi}{d\tau} = \sum_i \frac{\tilde{p}_i^2}{m_i s^3} - \frac{\tilde{g} kT}{s}. \tag{4}$$

Nosé [9] has shown that the dynamics associated with this system generate canonically distributed configurations, $\tilde{p}/s$ and q. To convert to real configurations, a noncanonical change of variables is used:

$$p = \frac{\tilde{p}}{s}, \qquad \hat{\pi} = \frac{\pi}{s}. \tag{5}$$

This is followed by a Sundman time transformation [20] applied to the vector field,

$$\frac{d\tau}{dt} = s, \tag{6}$$

resulting in a new system of non-Hamiltonian equations for the dynamics in the real variables:

$$\dot{q}_i = \frac{p_i}{m_i}, \qquad \dot{p}_i = -\frac{\partial}{\partial q_i} V(q) - p_i \frac{s\hat{\pi}}{Q}, \tag{7}$$

$$\dot{s} = \frac{s^2 \hat{\pi}}{Q}, \qquad \dot{\hat{\pi}} = \frac{1}{s}\left(\sum_i \frac{p_i^2}{m_i} - gkT \right) - \frac{s\hat{\pi}^2}{Q}. \tag{8}$$

Hoover [10] noted that the equations could be simplified considerably because $\hat{\pi}$ and s always appear together. By making another change of variables from $\hat{\pi}$ to $\xi = s\hat{\pi}/Q$ and from $\ln s$ to η, one not only eliminates the variable $\hat{\pi}$, but also decouples the variable s from the system. This results in the Nosé–Hoover equations for the dynamics in reduced real-variable formulation:

$$\dot{q}_i = \frac{p_i}{m_i}, \qquad \dot{p}_i = -\frac{\partial}{\partial q_i} V(q) - p_i \xi, \tag{9}$$

$$\dot{\eta} = \xi, \qquad \dot{\xi} = \frac{1}{Q}\left(\sum_i \frac{p_i^2}{m_i} - gkT \right). \tag{10}$$

In the reduced system the constant $g = N_f$ (the number of degrees of freedom of the real system) as opposed to $\tilde{g} = N_f + 1$ in the Nosé formulation. This reduction in the degrees of freedom is needed to recover configurations at the correct temperature [9]. Although this system is not Hamiltonian, it does have a conserved quantity, which we call the total extended energy:

$$E_{\text{ext}} = \sum_i \frac{p_i^2}{2m_i} + V(q) + \frac{Q\xi^2}{2} + gkT\eta. \tag{11}$$

The application of a Sundman time transformation necessarily destroys the canonical symplectic structure [26]. It is for this reason that the Nosé–Hoover system in (9)–(10) does not have such a structure.

This system is time-reversible, and it is advisable to solve the equations of motion with a reversible integrator. We will now explore two of the more commonly used reversible methods, both of which are based on variants of the generalized leapfrog algorithm [25].

The first is an implicit method [1] based on a modification of the velocity Verlet algorithm. It consists of alternating explicit and implicit half-steps with the momenta variables, with explicit whole-steps in the position variables. The method is given below in a whole-step formulation, i.e., as a mapping from time t_n to $t_{n+1} = t_n + \Delta t$:

$$p_i^{n+1/2} = p_i^n - \frac{\Delta t}{2}\left(\frac{\partial}{\partial q_i}V(q^n) + \xi^n p_i^n\right), \tag{12a}$$

$$\xi^{n+1/2} = \xi^n + \frac{\Delta t}{2Q}\left(\sum_i \frac{\left(p_i^n\right)^2}{m_i} - gkT\right), \tag{12b}$$

$$q_i^{n+1} = q_i^n + \Delta t \frac{p_i^{n+1/2}}{m_i}, \tag{12c}$$

$$\eta^{n+1} = \eta^n + \Delta t \xi^{n+1/2}, \tag{12d}$$

$$p_i^{n+1} = p_i^{n+1/2} - \frac{\Delta t}{2}\left(\frac{\partial}{\partial q_i}V(q^{n+1}) + \xi^{n+1} p_i^{n+1}\right), \tag{12e}$$

$$\xi^{n+1} = \xi^{n+1/2} + \frac{\Delta t}{2Q}\left(\sum_i \frac{\left(p_i^{n+1}\right)^2}{m_i} - gkT\right). \tag{12f}$$

Equations (12e) and (12f) are implicitly coupled and must be solved together. Traditionally, this step is solved with a $(3N + 1)$-dimensional Newton iteration [1]. This can be simplified considerably by substitution, eliminating p^{n+1} from the iteration. This results in a scalar–cubic equation in terms of ξ^{n+1} which can be solved either directly or using a simple iterative method.

Several explicit time-reversible methods have been proposed for the Nosé–Hoover equations [23–25]. The second method which we consider in this paper [23, 25] is one which is explicit and is based on the Störmer–Verlet method. We write it in its leapfrog form for comparison purposes:

$$p_i^{n+1/2} = p_i^n - \frac{\Delta t}{2}\left(\frac{\partial}{\partial q_i}V(q^n) + \xi^n p_i^{n+1/2}\right), \tag{13a}$$

$$q_i^{n+1} = q_i^n + \Delta t \frac{p_i^{n+1/2}}{m_i}, \tag{13b}$$

$$\xi^{n+1} = \xi^n + \frac{\Delta t}{Q}\left(\sum_i \frac{\left(p_i^{n+1/2}\right)^2}{m_i} - gkT\right), \tag{13c}$$

$$\eta^{n+1} = \eta^n + \frac{\Delta t}{2}(\xi^{n+1} + \xi^n), \tag{13d}$$

$$p_i^{n+1} = p_i^{n+1/2} - \frac{\Delta t}{2}\left(\frac{\partial}{\partial q_i}V(q^{n+1}) + \xi^{n+1} p_i^{n+1/2}\right). \tag{13e}$$

III. THE NOSÉ–POINCARÉ METHOD

As we illustrated in the previous section, the traditional real-variable formulation of Nosé–Hoover destroys the symplectic structure associated with the Nosé Hamiltonian. In this section we will outline a procedure for scaling time while preserving the Hamiltonian structure. The method proposed in this paper is formulated through a Poincaré transformation [20] of the Hamiltonian $\mathcal{H} = \mathcal{H}(q, p)$,

$$\tilde{\mathcal{H}} = f(q, p)(\mathcal{H} - \mathcal{H}_0), \qquad f > 0, \tag{14}$$

where f is a "time scaling" function, and the constant $\mathcal{H}_0$ is the initial value of $\mathcal{H}$. Along the energy slice $\mathcal{H} = \mathcal{H}_0$, the dynamics of the transformed system will be equivalent to those of the original system, up to a transformation of time. To see this, write the Hamilton equations of motion

$$\dot{q}_i = f \frac{\partial}{\partial p_i}\mathcal{H} + (\mathcal{H} - \mathcal{H}_0)\frac{\partial}{\partial p_i} f, \tag{15}$$

$$\dot{p}_i = -f \frac{\partial}{\partial q_i}\mathcal{H} - (\mathcal{H} - \mathcal{H}_0)\frac{\partial}{\partial q_i} f; \tag{16}$$

then observe that when $\mathcal{H} = \mathcal{H}_0$, the equations are the same as the original equations expressed in the real-time variable, t, related to τ by

$$\frac{d\tau}{dt} = f. \tag{17}$$

Now we consider the Poincaré transformation, $f = s$, applied to a slightly modified version of the Nosé extended Hamiltonian in (1):

$$\tilde{\mathcal{H}} = (\mathcal{H}_{\text{Nosé}} - \mathcal{H}_0)\, s, \tag{18}$$

$$\tilde{\mathcal{H}} = \left(\sum_i \frac{\tilde{p}_i^2}{2m_i s^2} + V(q) + \frac{\pi^2}{2Q} + gkT \ln s - \mathcal{H}_0 \right) s. \tag{19}$$

The modification comes in that we are using the constant $g = N_f$ (as opposed to $\tilde{g} = N_f + 1$). We will see later that this small change is necessary for the correct distribution of configurations. The constant $\mathcal{H}_0$ is chosen to be the initial value of the Nosé Hamiltonian, $\mathcal{H}_{\text{Nosé}}$. We will show that this transformed Hamiltonian in (2) and (19), which we call Nosé–Poincaré, generates configurations from the canonical distribution in the variables q and $\tilde{p}/s$.

THEOREM. *The Nosé–Poincaré system generates canonically distributed averages, given the usual statistical mechanics assumptions of equal a priori probabilities and ergodicity.*

The proof will involve derivation of the probability distribution, and partition function for the Nosé–Poincaré Hamiltonian.

Proof. Consider the probability of finding a particular configuration in the phase space described by the real variables (q, p):

$$dq\, dp F(q, p) \equiv \int d\pi \int ds\, d\tilde{p}\, dq\, F_{\text{ext}}(q, \tilde{p}, s, \pi)\,. \tag{20}$$

For the Nosé–Poincaré Hamiltonian, $\tilde{\mathcal{H}}$, we can write the probability of finding a particular configuration of energy $\tilde{\mathcal{H}}_0$ as a microcanonical distribution in the extended phase space $(q, \tilde{p}, s, \pi)$:

$$d\pi\, ds\, d\tilde{p}\, dq F_{\text{ext}}(q, \tilde{p}, s, \pi) = \frac{d\pi\, ds\, d\tilde{p}\, dq\, \delta[\tilde{\mathcal{H}} - \tilde{\mathcal{H}}_0]}{\int d\pi \int ds \int d\tilde{p} \int dq\, \delta[\tilde{\mathcal{H}} - \tilde{\mathcal{H}}_0]}. \tag{21}$$

In the above expression the usual statistical mechanical assumptions of equal *a priori* probabilities and ergodic (or quasi-ergodic) dynamics are made [27]. We now subsititute (21) in the expression (20), resulting in

$$dq\, dpF(q, p) = \frac{1}{\tilde{Z} N!\, h^{N_f}} \int d\pi \int ds\, d\tilde{p}\, dq\, \delta[\tilde{\mathcal{H}} - \tilde{\mathcal{H}}_0], \tag{22}$$

where the Nosé–Poincaré partition function is given by

$$\tilde{Z} = \frac{1}{N!\, h^{N_f}} \int d\pi \int ds \int d\tilde{p} \int dq\, \delta[\tilde{\mathcal{H}} - \tilde{\mathcal{H}}_0]. \tag{23}$$

Using $\tilde{\mathcal{H}}_0 = 0$, and expanding $\tilde{\mathcal{H}}$, we get

$$dq\, dpF(q, p) = \frac{1}{\tilde{Z} N!\, h^{N_f}} \int d\pi \int ds\, d\tilde{p}\, dq\, \delta[s(\mathcal{H}_{\text{Nosé}} - \mathcal{H}_0)]. \tag{24}$$

If we let $H(p, q) = \sum_i p_i^2/2m_i + V(q)$, this reduces to

$$dq\, dpF(q, p) = \frac{1}{\tilde{Z} N!\, h^{N_f}} \int d\pi \int ds\, d\tilde{p}\, dq\, \delta\left[s\left(H(\tilde{p}/s, q) + \frac{\pi^2}{2Q} + gkT \ln s - \mathcal{H}_0\right)\right]. \tag{25}$$

Because s is strictly positive, we can make the change of variables $p \leftarrow \tilde{p}/s$, yielding

$$dq\, dpF(q, p) = \frac{1}{\tilde{Z} N!\, h^{N_f}} \int d\pi \int ds\, dp\, dq\, s^{N_f} \delta\left[s\left(H(p, q) + \frac{\pi^2}{2Q} + gkT \ln s - \mathcal{H}_0\right)\right]. \tag{26}$$

Whenever a smooth function, $r(s)$, has a single simple root at $s = s_0$, one can write the relation $\delta[r(s)] = \delta[s - s_0]/|r'(s_0)|$. This relation can be directly applied to (26), resulting in

$$\begin{aligned} &\delta\left[s\left(H(p, q) + \frac{\pi^2}{2Q} + gkT \ln s - \mathcal{H}_0\right)\right] \\ &\quad = \frac{1}{|gkT|} \delta\left[s - \exp\left(\frac{-1}{gkT}\left(H(p, q) + \frac{\pi^2}{2Q} - \mathcal{H}_0\right)\right)\right]. \end{aligned} \tag{27}$$

These substitutions transform (26) into

$$\begin{aligned} &dq\, dp\, F(q, p) \\ &\quad = \frac{1}{\tilde{Z} N! h^{N_f}} \int d\pi \int ds\, dp\, dq\, \frac{s^{N_f}}{gkT} \delta\left[s - \exp\left(\frac{-1}{gkT}\left(H(p, q) + \frac{\pi^2}{2Q} - \mathcal{H}_0\right)\right)\right]. \end{aligned} \tag{28}$$

Integrating over s, and substituting for the root s_0, results in

$$dq\,dpF(q,p) = \frac{1}{\tilde{Z}N!\,h^{N_f}gkT}\exp\left(\frac{N_f\mathcal{H}_0}{gkT}\right)\int d\pi\,dq\,dp\exp\left(\frac{-N_f}{gkT}\left(H(p,q)+\frac{\pi^2}{2Q}\right)\right). \tag{29}$$

Finally, let $g = N_f$, and integrate over π to reduce the equation to

$$dq\,dpF(q,p) = \frac{C}{\tilde{Z}N!\,h^{N_f}}\,dq\,dp\exp\left(-\frac{1}{kT}H(p,q)\right), \tag{30}$$

where C is a positive constant. The above procedure can also be applied to $\tilde{Z}$, which can be then substituted along with (30) into (22). After canceling the prefactor $C/(N!\,h^{N_f})$ we have shown that

$$dq\,dpF(q,p) = \frac{dq\,dp\exp(-(1/kT)H(p,q))}{\int dq\int dp\exp(-(1/kT)H(p,q))}. \tag{31}$$

Because the right-hand side of the expression is the probability of finding a configuration in the canonical ensemble, this completes the proof. If, as is the usual case in molecular dynamics, total linear momentum is conserved, then an additional restriction of *zero* total linear momentum is required [9, 10, 28, 29]. ■

The disadvantage of the general Poincaré transformation in (14) is that it mixes the variables so that an explicit symplectic treatment of the extended Hamiltonian is not, in general, possible and one is compelled to use implicit symplectic methods (see [21, 22]). However, this is not always the case for transformation functions, f, which depend only on a reduced number of the phase-space variables (i.e., $f(q)$ or $f(s)$). In these special cases, the variables are sufficiently decoupled, and we can easily formulate explicit symplectic methods [16, 30].

Returning to the Nosé–Poincaré Hamiltonian, $\tilde{\mathcal{H}}$, we write the equations of motion

$$\dot{q}_i = \frac{\tilde{p}_i}{m_i s}, \qquad \dot{\tilde{p}}_i = -s\frac{\partial}{\partial q_i}V(q), \tag{32}$$

$$\dot{s} = s\frac{\pi}{Q}, \qquad \dot{\pi} = \sum_i \frac{\tilde{p}_i^2}{m_i s^2} - gkT - \Delta\mathcal{H}(q,\tilde{p},s,\pi), \tag{33}$$

$$\Delta\mathcal{H}(q,\tilde{p},s,\pi) = \sum_i \frac{\tilde{p}_i^2}{2m_i s^2} + V(q) + \frac{\pi^2}{2Q} + gkT\ln s - \mathcal{H}_0. \tag{34}$$

The value of $\mathcal{H}_0$ is chosen such that $\Delta\mathcal{H}(q_0,\tilde{p}_0,s_0,\pi_0) = 0$. A simple method for numerically solving the Nosé–Poincaré equations of motion is the generalized leapfrog algorithm [16, 30]. Because we are treating a Hamiltonian system, the resulting method is symplectic and time-reversible [13, 21, 22]:

$$\tilde{p}_i^{n+1/2} = \tilde{p}_i^n - \frac{\Delta t}{2}s^n\frac{\partial}{\partial q_i}V(q^n), \tag{35a}$$

$$\pi^{n+1/2} = \pi^n + \frac{\Delta t}{2}\left(\sum_i \frac{1}{m_i}\left(\frac{\tilde{p}_i^{n+1/2}}{s^n}\right)^2 - gkT\right) - \frac{\Delta t}{2}\Delta\mathcal{H}(q^n, \tilde{p}^{n+1/2}, s^n, \pi^{n+1/2}), \tag{35b}$$

$$s^{n+1} = s^n + \frac{\Delta t}{2}(s^{n+1} + s^n)\frac{\pi^{n+1/2}}{Q}, \tag{35c}$$

$$q_i^{n+1} = q_i^n + \frac{\Delta t}{2}\left(\frac{1}{s^{n+1}} + \frac{1}{s^n}\right)\frac{\tilde{p}_i^{n+1/2}}{m_i}, \tag{35d}$$

$$\pi^{n+1} = \pi^{n+1/2} + \frac{\Delta t}{2}\left(\sum_i \frac{1}{m_i}\left(\frac{\tilde{p}_i^{n+1/2}}{s^{n+1}}\right)^2 - gkT\right) - \frac{\Delta t}{2}\Delta\mathcal{H}(q^{n+1}, \tilde{p}^{n+1/2}, s^{n+1}, \pi^{n+1/2}), \tag{35e}$$

$$\tilde{p}_i^{n+1} = \tilde{p}_i^{n+1/2} - \frac{\Delta t}{2}s^{n+1}\frac{\partial}{\partial q_i}V(q^{n+1}). \tag{35f}$$

Due to the special structure of the system, the resulting method is also explicit. Note that (35b) requires the solution of a scalar quadratic equation for $\pi^{n+1/2}$,

$$\frac{\Delta t}{4Q}(\pi^{n+1/2})^2 + \pi^{n+1/2} + C = 0, \tag{36}$$

where

$$C = \frac{\Delta t}{2}\left(gkT(1 + \ln s^n) - \sum_i \frac{\left(\tilde{p}_i^{n+1/2}\right)^2}{2m_i(s^n)^2} + V(q^n) - \mathcal{H}_0\right) - \pi^n. \tag{37}$$

In this simplified formulation, C is a constant which can be easily computed. This equation can be solved explicitly using the quadratic formula, but one should be careful to solve for the correct root. To avoid subtractive cancellation in the computation, we use a variant of the quadratic formula to solve (36):

$$\pi^{n+1/2} = \frac{-2C}{1 + \sqrt{1 - C\Delta t/Q}}. \tag{38}$$

The remaining steps in the algorithm are completely explicit and can be solved sequentially.

IV. NUMERICAL EXPERIMENT: LENNARD–JONES FLUID

As a numerical experiment, we compare the two proposed Nosé–Hoover methods with the Nosé–Poincaré method. As a test problem, we consider 108 particles in cubic periodic box, using the minimum image convention. A truncated, shifted, and smoothed Lennard–Jones potential is used. It is important that the potential be smoothly truncated to zero to prevent artificial energy jumps [31]. Our experiments have indicated that the potential function should be at least $\mathcal{C}^2$; i.e., it has a continuous second derivative. We find this higher degree of smoothness to be important in some systems for verifying the order of the numerical

methods. The resulting smoothed pair potential function is

$$\tilde{V}_{LJ}(r) = \begin{cases} S(r)(V_{LJ}(r) - V_{LJ}(r_c)) & r \le r_c \\ 0 & r > r_c \end{cases}, \tag{39}$$

where

$$V_{LJ}(r) = 4\epsilon\left(\left(\frac{\sigma}{r}\right)^{12} - \left(\frac{\sigma}{r}\right)^{6}\right). \tag{40}$$

The smoothing function $S(r)$ is defined by

$$S(r) = 1 - 3\left(\frac{r}{r_c}\right)^2 + 3\left(\frac{r}{r_c}\right)^4 - \left(\frac{r}{r_c}\right)^6. \tag{41}$$

We give all of the results of our numerical experiments in reduced units. Specifically, we will use σ, ϵ, and m as the basic units of length, energy, and mass, respectively. In addition to the basic units, we will be using reduced temperature ($T^* = kT\epsilon^{-1}$), density ($\rho^* = \rho\sigma^3$), and time ($t^* = t\sigma\epsilon^{1/2}m^{-1/2}$). All of our simulations are performed with total linear momenta set to zero; hence we set $g = N_f$ with $N_f = 3N - 3$ (see [8, 28]). In all of the numerical experiments, we set the initial conditions of the extended variables to be $s^0 = 1$ and $\pi^0 = 0$. For this reason, the initial extended energy of the system is the same as the initial energy of the real system. We define the relative extended energy error at time t as

$$\left|\frac{E(t) - E(0)}{E(0)}\right|, \tag{42}$$

where the quantity E is determined by H, E_{ext}, and $\mathcal{H}_{\text{Nosé}}$ when using the Verlet, Nosé–Hoover, and Nosé–Poincaré methods, respectively (see Sections II and III for details).

In our first experiment, we start the simulation equilibrated to $T^* = 1.5$, with $\rho^* = 0.95$, and $Q = 1.0$. The timestep is set relatively low ($\Delta t^* = 0.005$), to verify the qualitative behavior of the methods in a numerically stable regime. In Fig. 1 the distribution of the

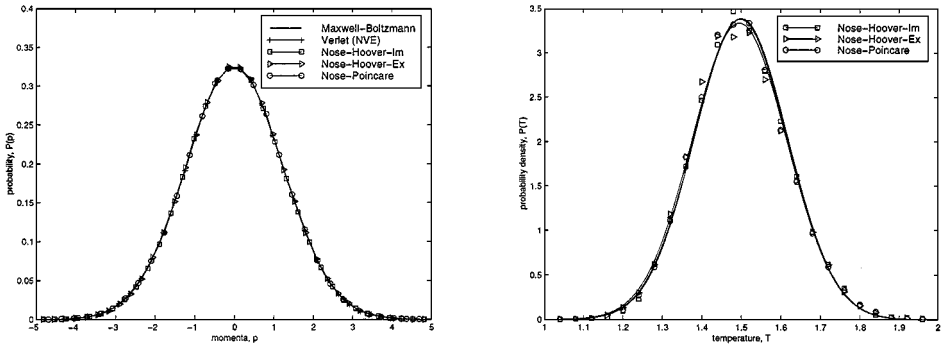

FIG. 1. Comparison of momenta and temperature distributions for a Lennard–Jones fluid ($N = 108$, $T^* = 1.5$, $\rho^* = 0.95$). The squares, triangles, circles, and pluses represent trajectories generated by the implicit Nosé–Hoover, explicit Nosé–Hoover, Nosé–Poincaré, and traditional Verlet methods, respectively. To the left, the momenta distribution is compared with the Maxwell–Boltzmann distribution (solid line). To the right, the distribution of the instantaneous temperature is shown. A Gaussian is fit to each curve to highlight the statistical similarities.

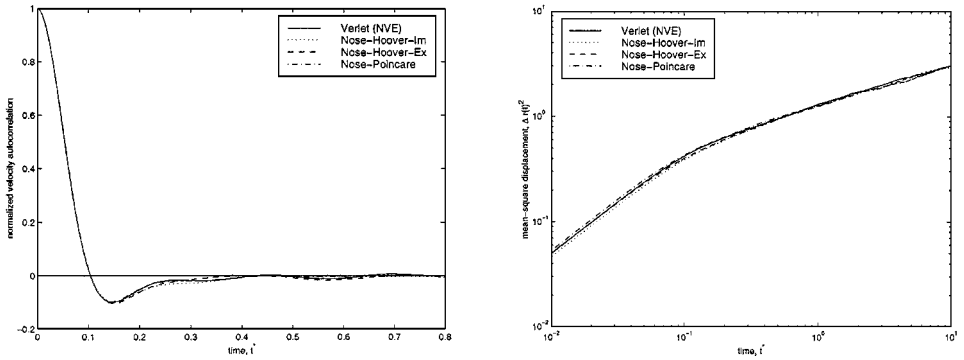

FIG. 2. Comparison of time-correlated quantities for a Lennard–Jones fluid ($N = 108$, $T^* = 1.5$, $\rho^* = 0.95$). The dotted, dashed, dashed–dotted, and solid lines represent trajectories generated by the implicit Nosé–Hoover, explicit Nosé–Hoover, Nosé–Poincaré, and traditional Verlet methods, respectively. To the left, the normalized velocity autocorrelation function $\frac{\langle v(t)\cdot v(0)\rangle}{\langle v(0)\cdot v(0)\rangle}$ is shown. To the right, the mean-square displacement is shown as a function of time.

momenta is compared with the Maxwell–Boltzmann distribution for this temperature. We also show the results from the Verlet method (traditional molecular dynamics), which does not use a temperature control. For this method, the simulation temperature cannot be determined until the simulation is complete. A tedious trial-and-error process had to be used to find initial conditions which would yield the correct temperature. This is why the Nosé methods are preferred to traditional molecular dynamics for generating configurations at constant temperature. As expected, all four methods generated Boltzmann distributed momenta, because the system is ergodic. We also show the distribution of the instantaneous temperature for the Nosé methods. All three generate Gaussian distributed temperatures with the same mean and variance.

We now investigate the behavior of the methods with respect to dynamical quantities associated with time-correlated functions. In Fig. 2 we show the velocity autocorrelation function and mean-square displacement as functions of time. All four methods give almost identical results for both of these functions. This indicates that the dynamics associated with Nosé–Hoover and Nosé–Poincaré evolve with the correct scale of time. We use the mean-square displacement curve to measure the diffusion coefficient and note that all four curves asymptotically approach straight lines of equal slope. Fitting a line to the curves in the asymptotic regime $t^* > 2.0$, we calculate the diffusion coefficient $D^* \approx 0.03$. To check the reliability of this estimate, we calculated the same value by numerical integration of the normalized autocorrelation curve. The two curves are related to eachother through the Einstein and Green–Kubo relations [32],

$$D = \frac{1}{2d}\lim_{t\to\infty}\frac{\Delta r^2(t)}{t} = \frac{kT}{m}\int_0^\infty \frac{\langle v(t)\cdot v(0)\rangle}{\langle v(0)\cdot v(0)\rangle}\,dt. \tag{43}$$

The parameter Q plays an interesting role in determining the characteristics of Nosé dynamics. In the limit as Q goes to infinity the extended variable s remains constant, and we recover traditional molecular dynamics. Similarly, one can verify that both the Nosé–Hoover and Nosé–Poincaré methods reduce to Verlet in this same limiting case. A drastically different situation arises when Q is small. This case is of practical interest because the rate at which configurational space is sampled can be increased by decreasing the size of Q.

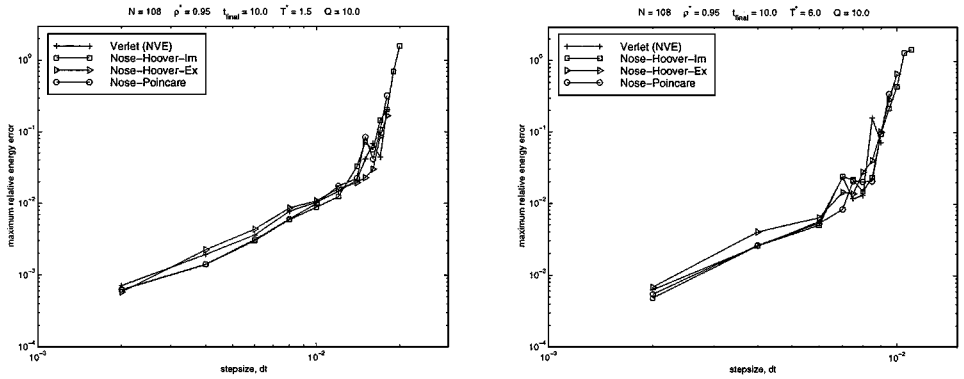

FIG. 3. Comparison of extended energy conservation as a function of stepsize for a Lennard–Jones fluid ($N = 108$ and $\rho^* = 0.95$). The maximum relative error in extended energy conservation is shown as a function of stepsize. A relatively large value for the "extended mass" is used ($Q = 10.0$). To the left, the curves are generated using a temperature of $T^* = 1.5$. To the right, a larger value, $T^* = 6.0$, is used.

However, one must be cautious not to make Q too small because this leads to high-frequency oscillations in s. This can lead to sampling problems, in addition to the computational difficulties. The best value for Q is problem dependent, and many authors have suggested that Q should be chosen in resonance with the real system to reduce "artificial effects" introduced by the thermostat [8–10, 29, 33, 34].

As a second test, we consider the effects of changes in the extended mass, Q, on the stability of the algorithms. We start with the case of a relatively large extended mass, $Q = 10$. Since the Nosé–Hoover and Nosé–Poincaré methods reduce to Verlet as Q becomes large, we expect similar behavior for all of the methods. Each simulation is started with the system properly equilibrated to the simulation temperature. We follow the dynamics for a range of stepsizes between 0.002 and 0.02 while the final time is held fixed at 10 units. In Fig. 3, the maximum relative error in the extended energy deviation is shown as a function of stepsize for two different temperatures, $T^* = 1.5$ and $T^* = 6.0$. For clarity, only the values in the stable regime of each method are shown in the diagram. The method was considered unstable if the simulation temperature deviated by more than 5% from the target value of $T^* = 1.5$ or $T^* = 6.0$. For this particular case, there is no clear difference in the efficiency of the methods. All four of the methods perform nearly the same for small stepsizes, as expected. However, for large stepsizes the implicit Nosé–Hoover method shows better stability properties. However, the magnitude of the error in the energy at the larger stepsizes is a concern, as it can be an indication of nonphysical behavior in the computed trajectory.

In Fig. 4, the same efficiency diagrams are shown for $Q = 0.1$. Since the Verlet method does not use the parameter Q, its results are the same as in the previous figure. For this smaller value of Q, the Nosé–Poincaré method is slightly more efficient than the explicit Nosé–Hoover method. Although the implicit Nosé–Hoover method shows better stability at large stepsizes, it is more inefficient than the other methods at smaller stepsizes. Our results indicate that the Nosé–Hoover methods are less efficient when the parameter Q is small. This could be a result of the more rapid fluctuations in the thermostat.

To further investigate the effect of fluctuations in the thermostat, we now consider the same system with a jump in the target temperature. The parameter Q is set to 0.1, and the simulation is started with the system equilibrated to $T^* = 1.5$ and $\rho^* = 0.95$. At $t^* = 0$ the Nosé thermostat is turned on, and the temperature is increased to $T^* = 6.0$. Due to the

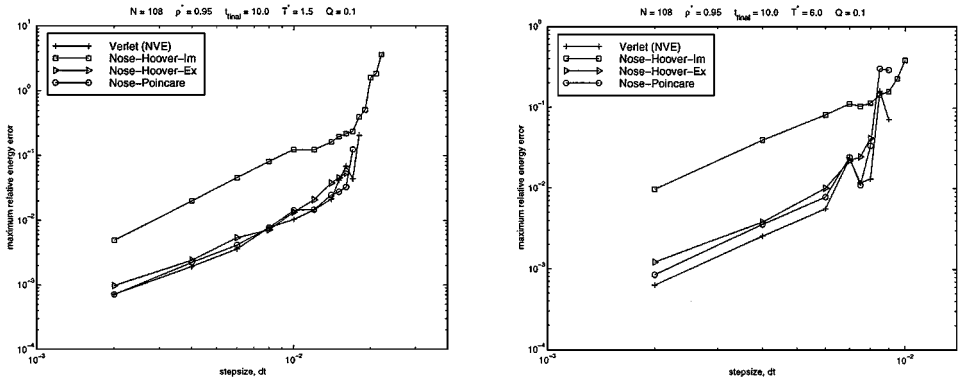

FIG. 4. Comparison of extended energy conservation as a function of stepsize for a Lennard–Jones fluid ($N = 108$ and $\rho^* = 0.95$). The maximum relative error in extended energy conservation is shown as a function of stepsize. A relatively small value for the "extended mass" is used ($Q = 0.1$). To the left, the curves are generated using a temperature of $T^* = 1.5$. To the right, a larger value, $T^* = 6.0$, is used.

change in the system temperature, we are unable to use traditional molecular dynamics algorithms (i.e., Verlet) for this simulation. In Fig. 5, the relative error in extended energy is shown as a function of stepsize. We also show the relative energy error for a particular stepsize, $\Delta t = 0.006$, near the stability limit. For all three of the algorithms, there is a large initial jump due to the increase in the imposed temperature. However, for large stepsizes the Nosé–Poincaré method is the most stable during this initial equilibration phase and shows the smallest jump in energy. For very small stepsizes, the explicit Nosé–Hoover method appears to be slightly more efficient than Nosé–Poincaré.

Over longer time intervals, the difference becomes even more pronounced. In our final experiment, we follow the dynamics for 500,000 steps at a stepsize of $\Delta t^* = 0.006$. The parameter Q is set to 0.1, and the simulation is started with the initial conditions equilibrated to the thermostat temperature of $T^* = 6.0$. In Fig. 6, the relative energy error is shown as a function of time. All of the methods show some drift in the energy for this long time simulation. However, the extended energy is conserved much better by the Nosé–Poincaré

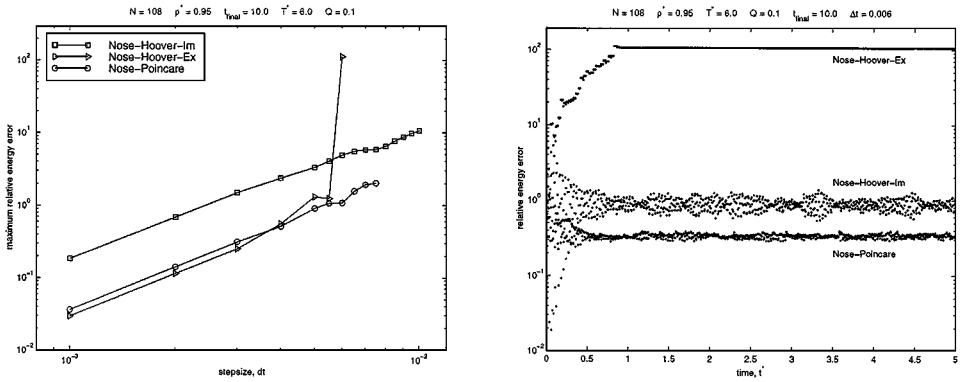

FIG. 5. Simulation of a temperature jump in a Lennard–Jones fluid ($N = 108$, $T^* = 6.0$, $\rho^* = 0.95$, $Q = 0.1$). The system was first equilibrated to $T^* = 1.5$ before the temperature was increased to $T^* = 6.0$ at $t^* = 0$. To the left, the maximum relative error in the extended energy is shown as a function of stepsize. To the right, the relative error in the extended energy is shown for a large stepsize ($\Delta t^* = 0.006$).

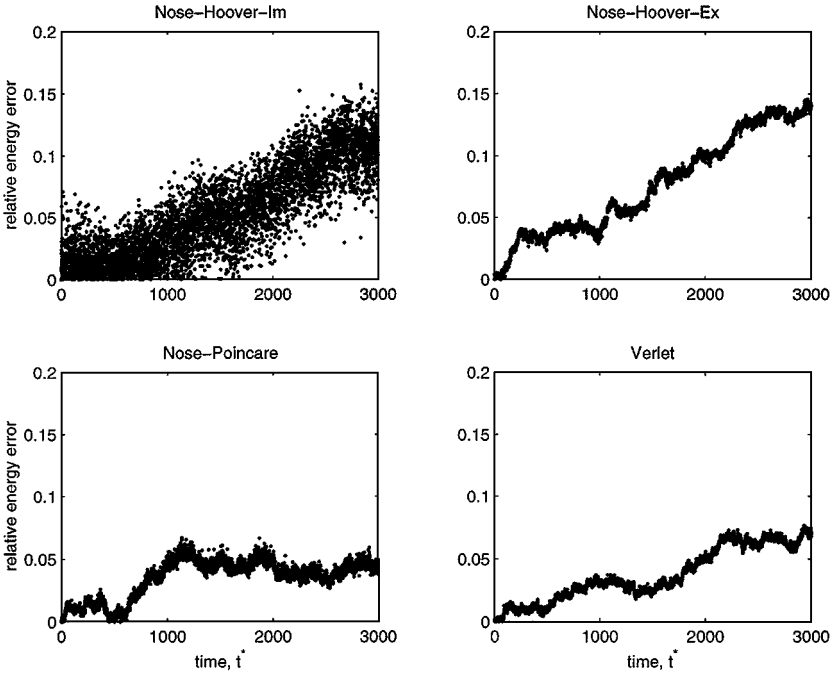

FIG. 6. Long time simulation of a Lennard–Jones fluid ($N = 108$, $T^* = 6.0$, $\rho^* = 0.95$, $Q = 0.1$). The dynamics was followed for 500,000 steps, at a stepsize of $\Delta t^* = 0.006$, with initial conditions equilibrated to $T^* = 6.0$. The relative error in the extended energy is shown as a function of stepsize for the various methods.

and Verlet methods. The Nosé–Hoover methods, which are not symplectic, are destabilized by the large fluctuations in temperature due to the small value of Q.

V. CONCLUSIONS

We have presented a new method for constant temperature (canonical) molecular dynamics, called Nosé–Poincaré. The new method has a wide range of applications, including rigid bodies and Nosé chains, while providing a symplectic framework for a real time formulation of the Nosé Hamiltonian. Although the traditional Nosé–Hoover approach also provides a real-variable system, it does so through a noncanonical change of variables. Both approaches are time reversible, but only Nosé–Poincaré has a canonical symplectic structure. Both time-reversible symmetry and symplecticness are strong geometric properties of a dynamical flow. The difference is in that the reversible symmetry of a numerical method does not, in general, provide an approximate integral obtainable through an asymptotic expansion of a "nearby Hamiltonian." Near conservation of energy over long time intervals is a direct result of this approximately conserved quantity. Although time-reversible methods will show the same type of stability near the symmetry plane ($p = 0$), there is no guarantee that this will be the case far from the symmetry plane ($|p| \gg 0$). This is one of the clear qualitative distinctions between symplectic and reversible methods.

Our numerical experiments have indicated that the Nosé–Poincaré formulation provides improved stability in simulations with large fluctuations in the thermostat variable. This situation arises when the initial temperature does not correspond to the simulation temperature

and when the parameter Q is small. In this case, the Nosé–Hoover methods show larger jumps in the extended energy for moderately large stepsizes. One should also note that our experiments have shown no clear difference between the explicit Nosé–Hoover method and Nosé–Poincaré for very small stepsizes, and when the system is properly equilibrated. The implicit Nosé–Hoover method is more stable at large stepsizes than the explicit form, but it is not as efficient in achieving a given degree of accuracy. Our observation is that for moderately large stepsizes the Nosé–Poincaré method can be a substantially better method and is certainly no worse than the Nosé–Hoover formulation. Because the Nosé–Poincaré method is symplectic, as well as time-reversible, we recommend its use for constant temperature simulations.

APPENDIX A: NOSÉ CHAINS

It has been shown that the Nosé Hamiltonian generates configurations from the canonical ensemble if the dynamics is ergodic [9, 10, 29]. The hypothesis of ergodicity can be violated in special cases [29, 34] (i.e., small systems and systems with stiff springs). A simple extension of the Nosé-Hoover equations has been developed, called Nosé–Hoover chains [33], which alleviates this ergodicity problem. This method involves introducing a sequence of new thermostats, each one coupled to the previous, resulting in a chain. The Nosé–Hoover chain equations are implicitly coupled, but can be solved explicitly using an even–odd splitting [24, 25]. To derive the equations for the chains, one starts with the Nosé–Hoover equations as defined in (9)–(10),

$$\dot{q}_i = \frac{p_i}{m_i}, \qquad \dot{p}_i = -\frac{\partial}{\partial q_i} V(q) - p_i \frac{\varphi}{Q}, \tag{A1}$$

$$\dot{\eta} = \frac{\varphi}{Q}, \qquad \dot{\varphi} = \sum_i \frac{p_i^2}{m_i} - gkT. \tag{A2}$$

Here the variable φ is equivalent to $Q\xi$ in Eqs. (9)–(10). Now $J-1$ new thermostats are introduced, each one coupled to the previous, resulting in a Nosé–Hoover chain:

$$\dot{q}_i = \frac{p_i}{m_i}, \qquad \dot{p}_i = -\frac{\partial}{\partial q_i} V(q) - p_i \frac{\varphi_1}{Q_1}, \tag{A3}$$

$$\dot{\eta}_1 = \frac{\varphi_1}{Q_1}, \qquad \dot{\varphi}_1 = \sum_i \frac{p_i^2}{m_i} - gkT - \varphi_1 \frac{\varphi_2}{Q_2}, \tag{A4}$$

$$\dot{\eta}_j = \frac{\varphi_j}{Q_j}, \qquad \dot{\varphi}_j = \frac{\varphi_{j-1}^2}{Q_{j-1}} - kT - \varphi_j \frac{\varphi_{j+1}}{Q_{j+1}}, \quad j = 2 \cdots J-1, \tag{A5}$$

$$\dot{\eta}_J = \frac{\varphi_J}{Q_J}, \qquad \dot{\varphi}_J = \frac{\varphi_{J-1}^2}{Q_{J-1}} - kT. \tag{A6}$$

While this system of equations is not Hamiltonian, there is a conserved quantity,

$$E_{\text{ext}} = \sum_i \frac{p_i^2}{2m_i} + V(q) + \sum_{j=1}^{J} \frac{\varphi_j^2}{2Q_j} + gkT\eta_1 + \sum_{j=2}^{J} \frac{\eta_j}{\beta}. \tag{A7}$$

This system is based on the time-reversible Nosé–Hoover system and is thus time-reversible. However, due to the noncanonical change of variables introduced by Nosé–Hoover, the resulting system has no Hamiltonian or symplectic structure. It has been rigorously proved [33] that the Nosé–Hoover chain equations generate configurations from the correct distribution, given that the dynamics is ergodic. This needed ergodicity is provided by the additional degrees of freedom in the chain of thermostats. The same idea can be applied directly to the Nosé Hamiltonian, resulting in *Nosé chains*:

$$\mathcal{H}_{\text{chain}} = \sum_i \frac{\tilde{p}_i^2}{2m_i s_1^2} + V(q) + \sum_{j=1}^{J-1} \frac{\pi_j^2}{2Q_j s_{j+1}^2} + \frac{\pi_J^2}{2Q_J} + gkT \ln s_1 + kT \sum_{j=2}^{J} \ln s_j. \quad \text{(A8)}$$

It is not obvious whether one can derive the Nosé–Hoover chain equations directly from the Nosé chain system. As in the case of a single thermostat, the real and intrinsic scales of time in the Nosé chain system are related by the scaling $d\tau/dt = s_1$. Because we are interested in capturing the correct timescale for the real variables, q and $\tilde{p}/s_1$, we apply a Poincaré transformation (see Section III) of the form

$$f = s_1 \quad \text{(A9)}$$

to the Nosé chain Hamiltonian in (A8). This results in a new Hamiltonian system which we call the Nosé–Poincaré chain,

$$\mathcal{H} = (\mathcal{H}_{\text{chain}} - \mathcal{H}_0)\, s_1. \quad \text{(A10)}$$

The constant $\mathcal{H}_0$ is chosen as the initial value of $\mathcal{H}_{\text{chain}}$. Since the rescaling variable s_1 is strictly positive, the quantity $\mathcal{H}_{\text{chain}}$ will be approximately conserved along the flow of $\mathcal{H}$. To formulate a numerical integrator for the Nosé–Poincaré chain system, we begin by writing out the equations of motion:

$$\dot{q}_i = \frac{\tilde{p}_i}{m_i s_1}, \qquad \dot{\tilde{p}}_i = -s_1 \frac{\partial}{\partial q_i} V(q), \quad \text{(A11)}$$

$$\dot{s}_1 = \frac{\pi_1 s_1}{Q_1 s_2^2}, \qquad \dot{\pi}_1 = \sum_i \frac{\tilde{p}_i^2}{m_i s_1^2} - gkT - \Delta\mathcal{H}(q, \tilde{p}, \vec{s}, \vec{\pi}), \quad \text{(A12)}$$

$$\dot{s}_j = \frac{\pi_j s_1}{Q_j s_{j+1}^2}, \qquad \dot{\pi}_j = \frac{\pi_{j-1}^2 s_1}{Q_{j-1} s_j^3} - \frac{kT s_1}{s_j}, \qquad j = 2 \cdots J-1, \quad \text{(A13)}$$

$$\dot{s}_J = \frac{\pi_J s_1}{Q_J}, \qquad \dot{\pi}_J = \frac{\pi_{J-1}^2 s_1}{Q_{J-1} s_J^3} - \frac{kT s_1}{s_J}, \quad \text{(A14)}$$

$$\Delta\mathcal{H}(q, \tilde{p}, \vec{s}, \vec{\pi}) = \mathcal{H}_{\text{chain}}(q, \tilde{p}, \vec{s}, \vec{\pi}) - \mathcal{H}_0. \quad \text{(A15)}$$

The new thermostats have introduced an implicit coupling to the equations of motion. One could solve this system using the generalized leapfrog algorithm, but in this case it would be an implicit method. To formulate an explicit method, we use a splitting of the Hamiltonian and corresponding Liouville operator. Although many choices for this splitting are possible, we will use an even–odd splitting [25] of the extended variables. For an odd

number of thermostats, J, this splitting results in three Hamiltonians:

$$\mathcal{H} = \mathcal{H}_1 + \mathcal{H}_2 + \mathcal{H}_3 \tag{A16}$$

$$\mathcal{H}_1 = \left(\sum_i \frac{\tilde{p}_i^2}{2m_i s_1^2} + \sum_{j=1} \frac{\pi_{2j}^2}{2Q_{2j}\, s_{2j+1}^2} + gkT \ln s_1 + kT \sum_{j=1} \ln s_{2j+1} \right) s_1 \tag{A17}$$

$$\mathcal{H}_2 = \left(\frac{\pi_1^2}{2Q_1 s_2^2} - \mathcal{H}_0 \right) s_1 \tag{A18}$$

$$\mathcal{H}_3 = \left(V(q) + \sum_{j=2} \frac{\pi_{2j-1}^2}{2Q_{2j-1} s_{2j}^2} + \frac{\pi_J^2}{2Q_J} + kT \sum_{j=1} \ln s_{2j} \right) s_1. \tag{A19}$$

To get a symplectic, time-reversible method, we use a symmetric splitting of the Liouville operator.

$$iL_{\mathcal{H}} = \{\cdot, \mathcal{H}\} = \{\cdot, \mathcal{H}_1\} + \{\cdot, \mathcal{H}_2\} + \{\cdot, \mathcal{H}_3\} = iL_1 + iL_2 + iL_3 \tag{A20}$$

In terms of the solution operator, this splitting introduces an error of order Δt^3 at each step, resulting in a second-order method:

$$\Psi_{\mathcal{H}}(\Delta t) = e^{(iL_{\mathcal{H}}\Delta t)} \tag{A21}$$

$$= e^{(iL_3\Delta t/2)} e^{(iL_2\Delta t/2)} e^{(iL_1\Delta t)} e^{(iL_2\Delta t/2)} e^{(iL_3\Delta t/2)} + O(\Delta t^3). \tag{A22}$$

Solving the dynamics of $\mathcal{H}_1$ and $\mathcal{H}_3$ for one step is straightforward because each s_j has been decoupled from its canonical momenta, π_j. On the other hand, the Hamiltonian $\mathcal{H}_2$ requires the solution of a quadratic, scalar differential equation for π_1 (which can be solved analytically). Once this is solved, its solution can be substituted into the equations for s_1 and π_2. Alternatively, one could solve $\mathcal{H}_2$ using the generalized leapfrog algorithm. Because the composition of symplectic maps is a symplectic map, this modification does not destroy the symplectic structure.

APPENDIX B: HOLONOMIC CONSTRAINTS AND RIGID BODIES

The formulation of Nosé–Poincaré with respect to a set of *arbitrary* holonomic constraints can be treated using an elementary modification of SHAKE discretization. Let us illustrate the treatment with the case of a single constraint, described in compact form by the Hamiltonian

$$\mathcal{H} = \left(\sum_i \frac{p_i^2}{2m_i s^2} + V(q) + \frac{\pi^2}{2Q} + gkT \ln s + \lambda \psi(q) - \mathcal{H}_0 \right) s. \tag{B1}$$

Here $\psi(q) = 0$ represents a constraint, and λ is the corresponding Lagrange multiplier.

The equations of motion of a general Hamiltonian system subject to constraints can be discretized using an extension of the SHAKE discretization [35], a natural generalization of the Verlet method. This method is second order and symplectic on the extended phase

space (see [36, 37]),

$$p_i^{n+1/2} = p_i^n - \frac{\Delta t}{2} s^n \left(\frac{\partial}{\partial q_i} V(q^n) + \lambda^n \frac{\partial}{\partial q_i} \psi(q^n) \right), \tag{B2}$$

$$\pi^{n+1/2} = \pi^n + \frac{\Delta t}{2} \left(\sum_i \frac{\left(p_i^{n+1/2}\right)^2}{2m_i (s^n)^2} - V(q^n) - \frac{(\pi^{n+1/2})^2}{2Q} - gkT(1 + \ln s^n) + \mathcal{H}_0 \right), \tag{B3}$$

$$s^{n+1} = s^n + \frac{\Delta t}{2}(s^{n+1} + s^n) \frac{\pi^{n+1/2}}{Q}, \tag{B4}$$

$$q_i^{n+1} = q_i^n + \frac{\Delta t}{2} \left(\frac{1}{s^{n+1}} + \frac{1}{s^n} \right) \frac{p_i^{n+1/2}}{m_i}, \tag{B5}$$

$$p_i^{n+1} = p_i^{n+1/2} - \frac{\Delta t}{2} s^{n+1} \left(\frac{\partial}{\partial q_i} V(q^{n+1}) + \lambda^{n+1} \frac{\partial}{\partial q_i} \psi(q^{n+1}) \right), \tag{B6}$$

$$\pi^{n+1} = \pi^{n+1/2} + \frac{\Delta t}{2} \left(\sum_i \frac{\left(p_i^{n+1/2}\right)^2}{2m_i (s^{n+1})^2} - V(q^{n+1}) - \frac{(\pi^{n+1/2})^2}{2Q} - gkT(1 + \ln s^{n+1}) + \mathcal{H}_0 \right), \tag{B7}$$

subject to the constraint

$$\psi(q^{n+1}) = 0. \tag{B8}$$

The equations can be efficiently solved using an iterative Newton algorithm. Extending the method to a vector of constraints is straightforward.

1. *Rigid Bodies*

We next consider the case of a system of rigid bodies subject to a Nosé-type thermostat. In particular, we are interested in applications such as typical molecular liquids where the rigid bodies are coupled only through the potential energy function V.

Often one sees this problem treated with separate thermostats for the translational and rotational motion [38]. We consider for simplicity the case of a system of rigid bodies on fixed centers, so there is only the rotational kinetic term and a single thermostat. Extensions to the case of multiple thermostats and translational motion can be derived in a straightforward manner [39].

We can easily describe the Hamiltonian in rotation matrix formulation, with $R_i = R_i(t) \in SO(3)$ an orthogonal matrix with unit determinant representing the orientation of the ith body. This results in a Hamiltonian description subject to the constraints $R_i^T R_i = E$, where E is the identity matrix. As described in [39–41], this is a more appropriate foundation than alternatives such as quaternions [38] or Euler angles for developing a geometric discretization of rigid body motion.

Denote by $\mathcal{T}_i^{\text{rot}}$ the rotational kinetic energy of the ith rigid body; then the Nosé Hamiltonian becomes

$$\mathcal{H} = \frac{1}{s^2} \sum_{i=1}^N \mathcal{T}_i^{\text{rot}} + V + \frac{1}{2Q} \pi_s^2 + gkT \ln s + \sum_{i=1}^N \operatorname{tr}\left(\left(R_i^T R_i - E \right) \Lambda_i \right), \tag{B9}$$

where the Λ_i are symmetric 3×3 matrix multipliers that are chosen to enforce the constraint relationships. $\mathcal{T}$ can be expressed in terms of the canonical momenta P, associated in the usual way to R (i.e., through partial derivatives of a Lagrangian with respect to $\dot{R}$). The kinetic term can also be described in terms of the angular momenta $\Pi_i = (\Pi_i^x, \Pi_i^y, \Pi_i^z)$ and the inertial tensor $I = \mathrm{diag}(I_x, I_y, I_z)$ by

$$\mathcal{T}_i^{\mathrm{rot}} = \frac{1}{2}\left(\frac{\left(\Pi_i^x\right)^2}{I_x} + \frac{\left(\Pi_i^y\right)^2}{I_y} + \frac{\left(\Pi_i^z\right)^2}{I_z}\right). \tag{B10}$$

The angular momenta then evolve, in the absence of the potential V, according to the Euler equations:

$$\frac{d}{dt}\Pi = \Pi \times I^{-1}\Pi. \tag{B11}$$

One method of treating this system is by applying the SHAKE discretization directly to the Hamiltonian in (B9) [42, 43]. Another approach is based on a splitting of the Hamiltonian. As described in [39–41], the unthermostatted system can be treated with a splitting method which solves alternately the kinetic term (in the angular momenta), then the potential term (in the rotation matrix formulation), with the different sets of variables coupled by appropriate linear transformations. The rotational terms can be reduced by a further splitting to several planar rotations. The resulting method is explicit, efficient, and easy to implement, and has been shown to behave very well in simulations of liquid water [39].

For the Nosé Hamiltonian, we must introduce the mechanism of a fictive time so that the integration timestep is properly adjusted according to fluctuations in energy. Second, an additional level of splitting of $\mathcal{H}$ is needed to compute the variable s. For this purpose, we introduce the Poincaré transformation as before,

$$\tilde{\mathcal{H}}_s = s(\mathcal{H} - \mathcal{H}_0) \tag{B12}$$

$$= \frac{1}{s}\sum_{i=1}^{N}\mathcal{T}_i^{\mathrm{rot}} + sV + \frac{s}{2Q}\pi_s^2 + gkTs\ln s + \sum_{i=1}^{N}\mathrm{tr}\left(\left(R_i^T R_i - E\right)\hat{\Lambda}_i\right) - \mathcal{H}_0 s, \tag{B13}$$

where we have rescaled the multiplier ($\hat{\Lambda}_i = s\Lambda_i$).

There are many ways to split $\tilde{\mathcal{H}}_s$. We use the natural three-way splitting into $\tilde{\mathcal{H}} = \mathcal{H}_1 + \mathcal{H}_2 + \mathcal{H}_3$, where

$$\mathcal{H}_1 = \frac{s}{2Q}\pi_s^2 + gkTs\ln s, \tag{B14}$$

$$\mathcal{H}_2 = \frac{1}{s}\sum_{i=1}^{N}\mathcal{T}_i^{\mathrm{rot}} + \frac{1}{2}\sum_{i=1}^{N}\mathrm{tr}\left(\left(R_i^T R_i - E\right)\hat{\Lambda}_i\right), \tag{B15}$$

and

$$\mathcal{H}_3 = +sV - \mathcal{H}_0 s + \frac{1}{2}\sum_{i=1}^{N}\mathrm{tr}\left(\left(R_i^T R_i - E\right)\hat{\Lambda}_i\right). \tag{B16}$$

The Hamiltonian $\mathcal{H}_1$ is a one degree of freedom system that is integrated using standard

methods. $\mathcal{H}_2$ can be reduced to the Euler equations for the free rigid bodies:

$$\frac{d}{dt}\Pi_i = \frac{1}{s}\Pi_i \times I^{-1}\Pi_i. \tag{B17}$$

$$\dot{\pi}_s = -\frac{1}{s^2}\sum_{i=1}^{N} \mathcal{T}_i^{\text{rot}}. \tag{B18}$$

We follow the approach introduced in [40, 41], treating this as a Hamiltonian system with Hamiltonian $\hat{H} = \frac{1}{2s}(\Pi_1^2/I_1 + \Pi_2^2/I_2 + \Pi_3^2/I_3)$ and the noncanonical Poisson structure defined by $\hat{J} = \text{skew}(\Pi)$. Noting that the Poisson bracket of s with $\hat{H}$ is zero, we see that an explicit Hamiltonian splitting method can be applied to give a symplectic integrator for Π. Note that this step must also include a trivial update of π_s. Finally, under $\mathcal{H}_3$, the momenta Π drift linearly in the direction of the tangent space projection of the gradient of V, and again π_s is subject to a simple update.

A symmetric splitting gives a second-order method. For example, we may solve successively each of the Hamiltonians $\frac{1}{2}\mathcal{H}_1$, $\frac{1}{2}\mathcal{H}_2$, $\mathcal{H}_3$, $\frac{1}{2}\mathcal{H}_2$, and $\frac{1}{2}\mathcal{H}_1$ for a step in time of length Δt. For additional details regarding the use of splitting, the reader is referred to [39–41] and the references therein.

ACKNOWLEDGMENTS

The authors were supported by NSF Grant DMS-9627330. Simulations were performed on computers provided by the Kansas Center for Advanced Scientific Computing and the Kansas Institute for Theoretical and Computational Science. The authors also thank Gregory Voth for stimulating conversations.

REFERENCES

1. D. Frenkel and B. Smit, *Understanding Molecular Simulation* (Academic Press, New York, 1996).
2. M. P. Allen and D. J. Tildesley, *Computer Simluation of Liquids* (Oxford Science, Oxford, UK, 1987).
3. H. C. Anderson, Molecular-dynamics simulations at constant pressure and–or temperature, *J. Chem. Phys.* **72**, 2384 (1980).
4. H. J. C. Berendsen, J. P. M. Postma, W. F. van Gunsteren, A. DiNola, and J. R. Haak, Molecular dynamics with coupling to an external bath, *J. Chem. Phys.* **81**, 3684 (1984).
5. D. J. Evans, Computer "experiment" for nonlinear thermodynamics of Coutte flow, *J. Chem. Phys.* **78**, 3297 (1983).
6. J. M. Haile and S. Gupta, Extensions of the molecular dynamics simulation method. II. Isothermal systems, *J. Chem. Phys.* **79**, 3067 (1983).
7. W. G. Hoover, A. J. C. Ladd, and B. Moran, High-strain-rate plastic flow studied via nonequilibrium molecular dynamics, *Phys. Rev. Lett.* **48**, 1818 (1982).
8. S. Nosé, A molecular-dynamics method for simluations in the canonical ensemble, *Mol. Phys.* **52**, 255 (1984).
9. S. Nosé, A unified formulation of the constant temperature molecular-dynamics methods, *J. Chem. Phys.* **81**, 511 (1984).
10. W. G. Hoover, Canonical dynamics: Equilibrium phase-space distributions, *Phys. Rev. A* **31**, 1695 (1985).
11. P. J. Olver, *Applications of Lie Groups to Differential Equations* (Springer-Verlag, New York, 1993), 2nd ed.
12. B. J. Leimkuhler, S. Reich, and R. D. Skeel, Integration methods for molecular dynamics, in *IMA Volumes in Mathematics and Its Applications* (Springer-Verlag, New York, 1996), Vol. 82, p. 161.
13. J. M. Sanz-Serna and M. P. Calvo, *Numerical Hamiltonian Problems* (Chapman and Hall, New York, 1995).
14. V. I. Arnold, *Mathematical Methods of Classical Mechanics* (Springer-Verlag, New York, 1978).

15. R. G. Winkler, V. Kraus, and P. Reineker, Time reversible and phase-space conserving molecular dynamics at constant temperature, *J. Chem. Phys.* **102**, 9018 (1995).
16. E. Hairer, Backward analysis of numerical integrators and symplectic methods, *Ann. Numer. Math.* **1**, 107 (1994).
17. G. Benettin and A. Giorgilli, On the Hamiltonian interpolation of near to the identity symplectic mappings with application to symplectic integration algorithms, *J. Statist. Phys.* **74**, 1117 (1994).
18. G. R. W. Quispel and J. A. G. Roberts, Chaos and time-reversal symmetry, *Phys. Rep.* **216**, 63 (1992).
19. B. Mehlig, D. W. Heermann, and B. M. Forest, Hybrid Monte Carlo method for condensed matter systems, *Phys. Rev. B* **45**, 679 (1992).
20. K. Zare and V. Szebehely, Time transformations for the extended phase space, *Celestial Mech.* **11**, 469 (1975).
21. E. Hairer, Variable time step integration with symplectic methods, *Appl. Numer. Math.* **25**, 219 (1997).
22. S. Reich, Backward error analysis for numerical integrators, submitted for publication.
23. B. L. Holian, A. J. De Groot, W. G. Hoover, and C. G. Hoover, Time-reversible equilibrium and nonequilibrium isothermal–isobaric simulations with centered-difference Stoermer algorithms, *Phys. Rev. A* **41**, 4552 (1990).
24. G. J. Martyna, M. E. Tuckerman, D. J. Tobias, and M. L. Klein, Explicit reversible integrators for extended systems dynamics, *Mol. Phys.* **87**, 1117 (1996).
25. S. Jang and G. A. Voth, Simple reversible molecular dynamics algorithms for Nosé-Hoover chain dynamics, *J. Chem. Phys.* **107**, 9514 (1997).
26. D. Stoffer, Variable steps for reversible methods, *Computing* **55**, 1 (1995).
27. D. A. McQuarrie, *Statistical Mechanics* (Harper and Row, New York, 1976).
28. T. Çağin and J. R. Ray, Isothermal molecular-dynamics ensembles, *Phys. Rev. A* **37**, 4510 (1988).
29. S. Nosé, Constant temperature molecular dynamics methods, *Prog. Theor. Phys. Supp.* **103**, 1 (1991).
30. Geng Sun, Symplectic partitioned Runge–Kutta methods, *J. Comput. Math.* **11**, 365 (1993).
31. R. J. Loncharich and B. R. Brooks, The effects of truncating long-range forces on protein dynamics, *Proteins* **6**, 32 (1989).
32. J. P. Hansen and I. R. McDonald, *Theory of Simple Liquids* (Academic Press, New York, 1986), 2nd ed.
33. G. J. Martyna, M. L. Klein, and M. Tuckerman, Nosé–Hoover chains: The canonical ensemble via continuous dynamics, *J. Chem. Phys.* **97**, 2635 (1992).
34. S. Toxvaerd and O. H. Olson, Molecular dynamics at constant temperature, *Physica Scripta T* **T33**, 98 (1990).
35. J. P. Ryckaert, G. Ciccotti, and H. J. C. Berendsen, Numerical integration of the cartesian equations of motion of a system with constraints: Molecular dynamics of n-alkanes, *J. Comput. Phys.* **23**, 327 (1977).
36. B. Leimkuhler and R. Skeel, Symplectic numerical integrators in constrained Hamiltonian systems, *J. Comput. Phys.* **112**, 117 (1994).
37. L. O. Jay, Symplectic partitioned Runge–Kutta methods for constrained Hamiltonian systems, *SIAM J. Numer. Anal.* **33**, 368 (1996).
38. A. Bulgac and M. Adamuti-Trache, Molecular dynamics of rigid molecules, *J. Chem. Phys.* **105**, 1131 (1996).
39. A. Dullweber, B. Leimkuhler, and R. McLachlan, A symplectic splitting method for rigid-body molecular dynamics, *J. Chem. Phys.* **107**, 5840 (1997).
40. R. I. McLachlan, Explicit Lie–Poisson integration and the Euler equations, *Phys. Rev. Lett.* **71**, 3043 (1993).
41. S. Reich, Momentum conserving symplectic integrators, *Physica D* **76**, 375 (1994).
42. A. Kol, B. B. Laird, and B. J. Leimkuhler, A symplectic method for rigid-body molecular simulation, *J. Chem. Phys.* **107**, 2580 (1997).
43. R. I. McLachlan and C. Scovel, Equivariant constrained symplectic integration, *J. Nonlinear Sci.* **5**, 233 (1995).